Title
Investigating Lithium-Ion Batteries using Low-Field Nuclear Magnetic Resonance and Relaxometry: A Short Story

Author
Martinez, Samuel R

Publication Date
2021

Peer reviewed|Thesis/dissertation

Investigating Lithium-Ion Batteries using Low-Field Nuclear Magnetic Resonance and Relaxometry: A Short Story

By

SAM MARTINEZ

THESIS

Submitted in partial satisfaction of the requirements for the degree of

MASTER OF SCIENCE

in

Chemistry

in the

OFFICE OF GRADUATE STUDIES

of the

UNIVERSITY OF CALIFORNIA

DAVIS

Approved:

Matthew Augustine, Chair

Dylan Murray

Donald Land

Committee in Charge

2022

Acknowledgments

Well… what a ride. I have made some of the best friends during my time here in Davis, including, and maybe most unexpectedly, my boss. Previous work experiences have ingrained in me this sense that bosses are really just around to nag you to do more without wanting to pay you more, and not caring about you as a person in general. Then, here comes this wild looking dude one day slammin' a beer while giving his presentation to the first-year grad students about his lab. Fast-forward to me joining Matt's lab, and our average conversation isn't, "Hey, can you work more," but, "Hey, let's grab our Harley's and hit the road this weekend. Bring the whiskey." I couldn't have asked for a better boss, Matt Augustine. Oh, and I learned some shit about NMR along the way too.

With a badass boss comes a pretty awesome lab too: Dan, Julia, Brandon, Sophia, Vanessa, Matty and Javier. I want to thank all of you for the experiences we shared at UC Davis. From our hour and a half long lunches at Raj's, to shooting guns at the gun range (or in nature), to our Friday night game nights, I'll always remember these times and what they meant to me.

Next, I want to give a quick shout-out to Dr. Dylan Murray. From my first year here when we talked about NMR, to taking your enjoyable CHE 216 class and even through TA'ing for you, I've always thought highly of you and appreciated your sense of humor.

Thank you everyone for the memories.

Table of Contents:

Abstract

Lithium-ion batteries provide lightweight, energy dense, and efficient power for portable electronics and electric vehicles. Accompanying the rise of lithium battery technology is the need for fast, non-destructive diagnostic techniques to determine important battery performance or safety parameters. Low-field NMR and relaxometry is an ideal technique to probe lithium-ion polymer (LiPo) batteries due to its ability to penetrate the aluminum casing of these batteries. The development of a few different low-field techniques are presented here to measure different battery parameters. This includes measuring the T_1 and T_2 relaxation times of LiPo batteries at differing states of charge, magnetic resonance imaging showing T_2 as a function of position across a battery, and using pulsed field gradient ^{7}Li nuclear magnetic resonance (NMR) to measure Li diffusion coefficients.

Chapter 1: Nuclear Magnetic Resonance Theory

1.1 Introduction

Nuclear Magnetic Resonance (NMR) spectroscopy is a powerful tool for the spectroscopist. NMR can be used to determine molecular structure of various molecules, measure relaxation times, study diffusion, image a variety of samples in multi-dimensions, and has as much potential as one's creativity dictates [1-4]. This collection of pages will include the theory of NMR using classical and quantum mechanical approaches designed to simplify the phenomenon of nuclear induction so that all may understand its splendor. The classical mechanics of the interactions between 'spin,' the mysterious quantum mechanical facet, and electromagnetic fields tends to be more easily digested, and as such, will be the start of this chapter. From there, a quantum mechanical view will be taken where the similarities will be highlighted between the two approaches.

1.2 Classical Dynamics: The Bloch Equations

Nuclei with spin values greater than zero interact with magnetic fields. In the macroscopic sense, these nuclei can be viewed as a collection of magnetic dipoles. The sum of the magnetic moment vectors, $\vec{\mu}$, of these dipoles in the absence of a magnetic field, $\vec{B}$, results in a net zero bulk magnetic moment, $\vec{M}$, according to Eqn. 1.1.

$$\boldsymbol{M} = \sum_i \boldsymbol{\mu}_i \tag{1.1}$$

Yet, in the presence of a magnetic field, the magnetic moments of the nuclei either align with or against the external magnetic field to achieve thermal equilibrium as seen in Fig. 1. (This will be discussed in further detail in later chapters).

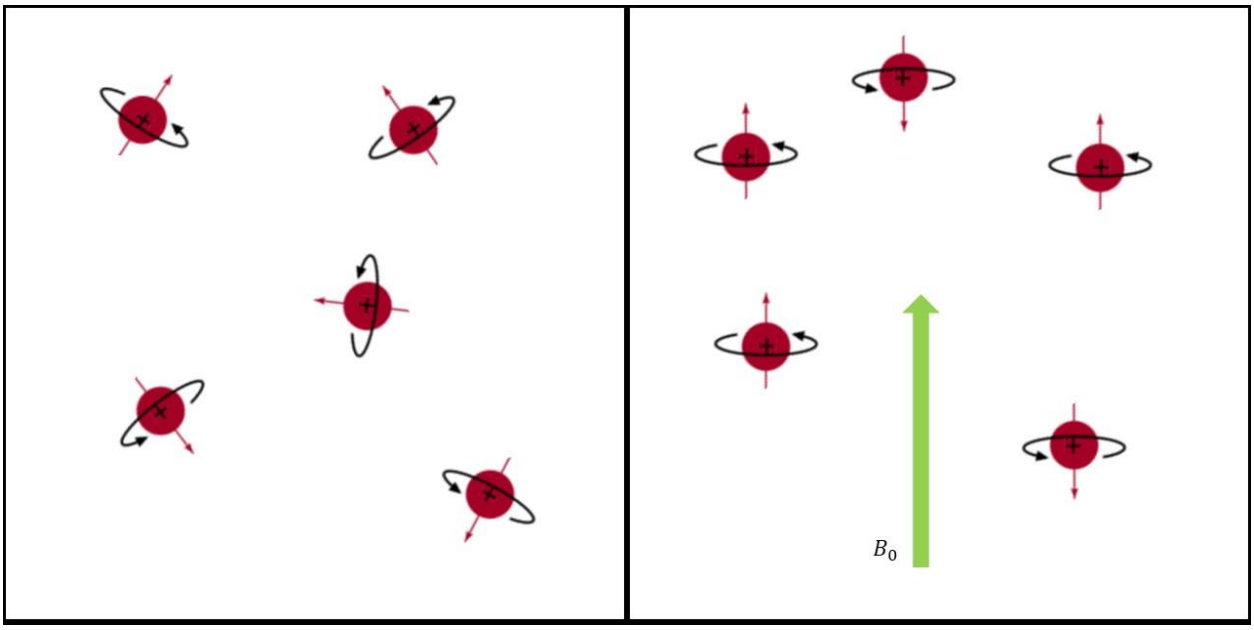

Figure 1.1. Illustration depicting nuclear spins randomly aligned in the absence of an external magnetic field $\vec{B}$ (left), and aligned parallel and antiparallel with B_0, the z component of $\vec{B}$ (right).

The equations of motion that govern this process are known as the Bloch equations derived by Felix Bloch in 1946 as a classical and macroscopic approach to describe the lineshape of a simple NMR spectrum [5].

The total magnetic moment of a sample, or magnetization $\boldsymbol{M}$, is the summation over all individual magnetic moments in the sample as seen in Eqn. 1.1. In terms of the total spin angular momentum $\boldsymbol{P}$, Eqn. 1.1 can be written as,

$$\boldsymbol{M} = \gamma \boldsymbol{P} \quad \textbf{(}1.2\textbf{)}$$

where γ is the ratio between the magnetic moment and the angular momentum and is known as the gyromagnetic ratio. The interaction of an applied magnetic field and the magnetization results in a torque on the system which changes the angular momentum $\boldsymbol{P}$.

$$\frac{d}{dt}\boldsymbol{P} = \boldsymbol{M} \times \boldsymbol{B} \quad (1.3)$$

We see that $\boldsymbol{P}$ and $\boldsymbol{M}$ are related by Eqn. 1.2 so we can write,

$$\frac{d}{dt}\boldsymbol{M} = \gamma[\boldsymbol{M} \times \boldsymbol{B}] \quad (1.4)$$

The classical motion of the individual nuclear moments $\boldsymbol{\mu}$ in a sample are described by a similar equation. The steady-state solution of which is a precession of the system of moments around the applied field direction with angular velocity $\boldsymbol{\omega}_0 = \gamma \boldsymbol{B}_0$**.** This is known as the Larmor precession or frequency, where the frequency would be $\gamma B/2\pi$.

When placed in a magnetic field B_0, the bulk magnetic moment of the sample will change from a net zero moment to M_0, the equilibrium value of magnetization. The equation of motion for the magnetization of the sample must include the Larmor precession as well as the shift to an equilibrium value of magnetization as it approaches thermal equilibrium. The approach to thermal equilibrium is known as relaxation with characteristic time constants T_1 and T_2. Bloch posited that

this relaxation decayed exponentially with components parallel and perpendicular to $\boldsymbol{M}_0$. Adding this relaxation phenomenon to Eqn. 1.4 gives

$$\begin{aligned}\frac{d}{dt}M_x &= \gamma[\boldsymbol{M}\times\boldsymbol{B}]_x - \frac{M_x}{T_2}\\ \frac{d}{dt}M_y &= \gamma[\boldsymbol{M}\times\boldsymbol{B}]_y - \frac{M_y}{T_2}\\ \frac{d}{dt}M_z &= \gamma[\boldsymbol{M}\times\boldsymbol{B}]_z - \frac{(M_z-M_0)}{T_1}\end{aligned} \qquad (1.5)$$

A brief summary of relaxation is provided later in this chapter and a more extensive dive into the theory of relaxation occurs in Ch. 3.

1.2.1 Applying a Radio Frequency Field

Now, suppose a linearly polarized radio frequency (RF) field, $\boldsymbol{B}_{rf} = B_1\cos(\omega t)\hat{\boldsymbol{\imath}}$ is applied to the system of spins that make up the sample. This oscillating component of the RF field can be resolved into two components rotating in opposite directions with an angular frequency ±ω. Only the component rotating in the same direction as the Larmor precession (+ω) will be considered. In the presence of a static magnetic field the magnetization in the transverse plane will be rotating around the $+z$ direction with angular frequency ω. With the addition of the $\boldsymbol{B}_1$field, the $\boldsymbol{B}$ field experienced by the sample becomes,

$$\boldsymbol{B} = B_1\cos(\omega t)\,\hat{\boldsymbol{\imath}} + B_1\sin(\omega t)\,\hat{\boldsymbol{\jmath}} + B_0\hat{\boldsymbol{k}} \qquad (1.6)$$

where $\hat{\boldsymbol{\imath}}, \hat{\boldsymbol{\jmath}}$, and $\hat{\boldsymbol{k}}$ are unit vectors in the x, y, and z directions. Now, inserting the new magnetic field exerted upon our spins as expressed in Eqn. 1.6 with the free precession and relaxation terms in Eqn. 1.5, we get the Bloch equations:

$$\begin{aligned} \frac{d}{dt}M_x &= \gamma\left[B_1 \sin(\omega t)\, M_z + B_0 M_y\right] - \frac{M_x}{T_2} \\ \frac{d}{dt}M_y &= -\gamma[B_0 M_x - B_1 \cos(\omega t) M_z] - \frac{M_y}{T_2} \\ \frac{d}{dt}M_z &= -\gamma\left[B_1 M_x \sin(\omega t) + B_1 M_y \cos(\omega t)\right] - \frac{(M_z - M_0)}{T_1} \end{aligned} \tag{1.7}$$

Neglecting the relaxation terms for the moment, it is simple to show the solution to these equations under the condition $\boldsymbol{M}(t) = M_0\boldsymbol{k}$, is

$$\begin{aligned} M_x &= M_0 sin(\omega_1 t) sin(\omega_0 t) \\ M_y &= M_0 sin(\omega_1 t) cos(\omega_0 t) \\ M_z &= M_0 cos(\omega_1 t) \end{aligned} \tag{1.8}$$

where $\omega_1 = \gamma B_1$. Eqn. 1.8 implies that when a RF field of frequency ω_0 is applied transverse to the large, static magnetic field, B_0, the net magnetization vector precesses about B_0 (+ z-axis) at a frequency ω_0 and about the RF field B_1 at a frequency ω_1 as seen in Fig. 1.2.

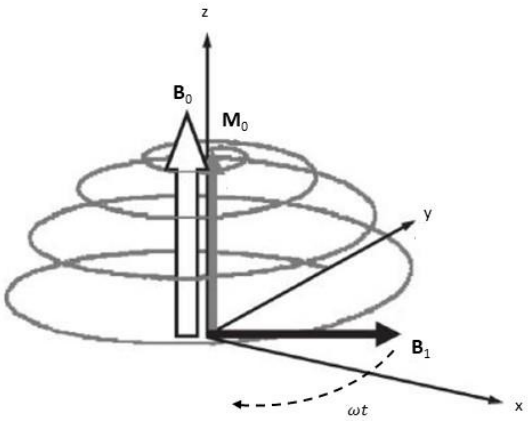

Figure 1.2. The trajectory of the nuclear spin magnetization in the laboratory frame of reference when a transverse $\boldsymbol{B}_1$ field is applied. When $\omega = \omega_0$ the net magnetization precesses about both $\boldsymbol{B}_0$ at frequency ω_0 and about $\boldsymbol{B}_1$ at frequency ω_1.

1.2.2 The Rotating Frame of Reference

If the frame of reference were to change to be rotating with the $\boldsymbol{B}_1$ field about $\boldsymbol{B}_0$, then $\boldsymbol{B}_1$ would appear to be stationary and there would only be precession about $\boldsymbol{B}_1$ at a frequency of ω_1. This new frame of reference is known as the *rotating frame*.

After a small magnetic field $\boldsymbol{B}_1$ is applied transverse to the static magnetic field, the net magnetization will not start to precess about the z-axis in the rotating frame because the static B_0 field has been effectively removed when on resonance ($\omega_0 = \omega$). Instead, the precessional motion of $\boldsymbol{M}_0$ (i.e. $\omega_0 = \gamma B_0$) in the rotating frame is reduced to ($\omega_0 - \omega$), known as the offset frequency Ω, which corresponds to precession in an apparent field $(\omega_0 - \omega)/\gamma \equiv B_0(1 - \omega_0/\omega)$. This means that the residual field ΔB_0 along the z-axis in the rotating frame is $\Delta B_0 = \Omega/\gamma$ which vanishes if $\omega = \omega_0$. If the resonance offset Ω is non-zero, then there will be some effective field $\boldsymbol{B}_{eff}$ in the rotating frame and $\boldsymbol{M}_0$ will precesses about $\boldsymbol{B}_{eff}$ in that frame. The motion of

magnetization, neglecting relaxation, in the rotating frame about an effective field can be seen in Figure 1.3 for two cases of offset frequency.

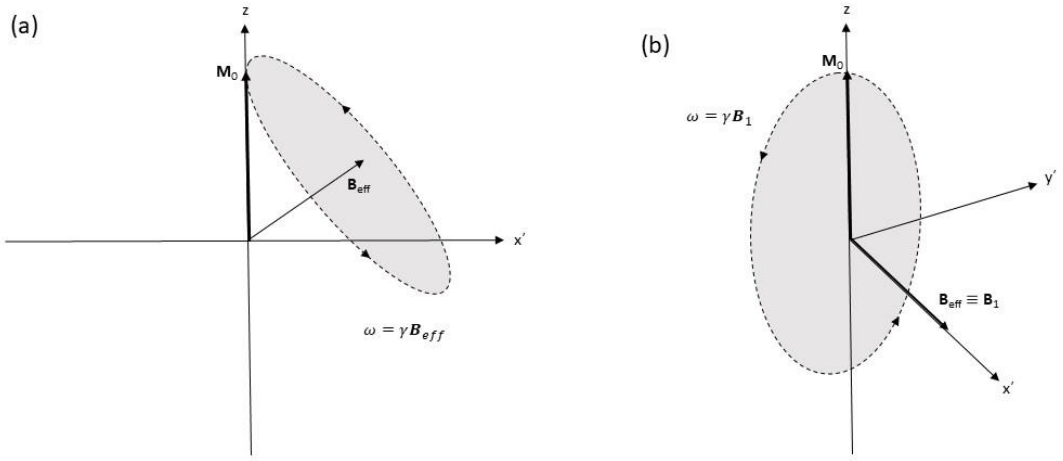

Figure 1.3. Effective fields and precessional motion of the magnetization vector $\boldsymbol{M}_0$ in the rotating frame with an applied radio frequency pulse ω_1 (a) below resonance and (b) on resonance.

To simplify the Bloch equations further, we will apply this concept of the *rotating frame of reference* to Eqn. 1.7. In a static magnetic field B_0 along the z direction the transverse magnetization M_{xy} will rotate around the z axis with an angular velocity ω_0. If an observer were to rotate at some angular velocity ω in the same direction, then M_{xy} would appear to move as $\omega_0 - \omega$. If the observer rotated at exactly ω_0 then the M_{xy} magnetization would appear stationary. We will let x, y, z be the cartesian coordinates for the lab frame (or stationary frame) of reference while x', y', z' will represent the rotating frame of reference which is rotating around the z ($z = z'$) axis

of the lab frame at angular velocity ω. So, how does the transverse magnetization act in the rotating frame of reference? To find out, lets transform to the rotating frame by applying a rotation matrix to $\boldsymbol{M}$.

$$\begin{bmatrix} \cos(\omega t) & -\sin(\omega t) & 0 \\ \sin(\omega t) & \cos(\omega t) & 0 \\ 0 & 0 & 1 \end{bmatrix} \cdot \begin{bmatrix} M_x \\ M_y \\ M_z \end{bmatrix} = \begin{bmatrix} M_x \cos(\omega t) - M_y \sin(\omega t) \\ M_x \sin(\omega t) + M_y \cos(\omega t) \\ M_z \end{bmatrix} = \begin{bmatrix} M'_x \\ M'_y \\ M'_z \end{bmatrix} \tag{1.9}$$

Now, to find the equation of motion for M'_{xy} with respect to time we will differentiate Eqn. 1.9 and substitute in Eqn. 1.7 to reveal the Bloch equations in the rotating frame

$$\begin{aligned} \frac{d}{dt} M'_x &= \Omega M'_y - \frac{M'_x}{T_2} \\ \frac{d}{dt} M'_y &= \Omega M'_x - \frac{M'_y}{T_2} + \omega_1 M_z \\ \frac{d}{dt} M'_z &= -\omega_1 M'_y - \frac{M_z - M_0}{T_1} \end{aligned} \tag{1.10}$$

where Ω is the offset frequency equal to $\omega_0 - \omega$, $\omega_0 = \gamma B_0$ is the Larmor frequency precessing around B_0, and $\omega_1 = \gamma B_1$ is the nutation frequency.

1.2.3 Pulsed NMR

Most modern NMR spectrometers employ pulsed magnetic resonance techniques. In pulsed NMR the RF field is turned on for a short period, usually anywhere from 1 μs to 60 μs, which is short relative to T_1 and T_2 times (on the order of milliseconds) and is then turned off

again. The B_1 field applied is set sufficiently closely to the resonance frequency of the nucleus of interest so that the RF pulse exerts a torque on the net magnetization in the rotating frame.

Upon applying a RF pulse in the rotating frame of reference, the nuclear magnetization, $\boldsymbol{M}_0$, will precess at a rate of $\omega_1 = \gamma B_1$ around the effective magnetic field (Fig. 1.3). The stronger the applied RF pulse, the faster the precession occurs. Eventually, the resonant RF pulse flips the net magnetization into the transverse plane (known as a 90° pulse) according to the equation $\beta = \omega_1 \tau_p$, where β equals the flip angle from the $+z$ axis (the direction of $\boldsymbol{B}_0$), ω_1 equals the angular frequency of the pulse, and τ_p equals the RF pulse time. After a time twice as long, the net magnetization will lie along the $-z$ direction (known as a 180° pulse). By letting β equal $\frac{\pi}{2}$ we can find a set value for τ_p ($\tau_p = \frac{\pi}{2\gamma B_1}$) where $\boldsymbol{M}_0$ will have been turned through 90°. The use of strong RF pulses allows us to position the magnetization in any direction we choose without any decrease in magnitude of $\boldsymbol{M}_0$ as long as the RF pulse time (τ_p) is significantly smaller than T_1 or T_2. This effect can be seen in Figure 1.4.

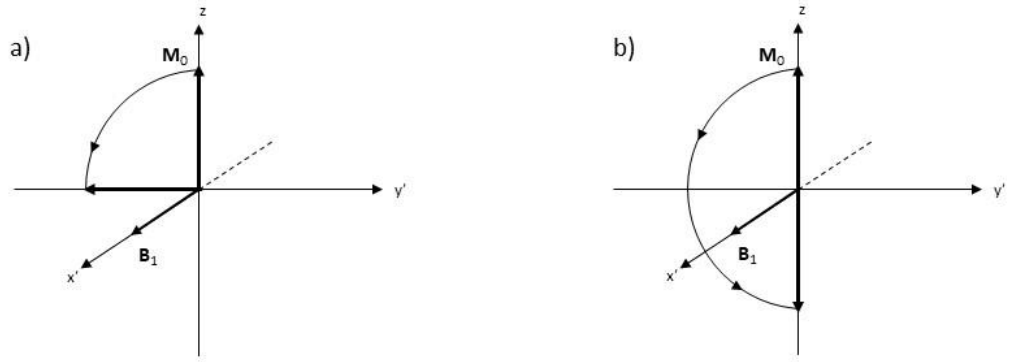

Figure 1.4. The effects of a 90° RF pulse (a) and a 180° RF pulse (b) on the net magnetization $\boldsymbol{M}_0$, in the rotating frame of reference.

1.2.4 Relaxation

To this point, we have neglected the relaxation terms when describing the Bloch equations and when discussing RF pulses. This phenomenon will be addressed here briefly while a more extensive look at the theory of relaxation will be provided in Ch. 3.

The purpose of an RF pulse is to perturb the spin system from thermal equilibrium. Macroscopically, this looks like applying a RF pulse to the system to shift the M_0 magnetization away from its equilibrium position along the static magnetic field B_0 direction (Fig. 1.4). After the pulse, the magnetization will be restored to its equilibrium position through a process called spin-lattice or longitudinal relaxation. The phenomenological description of this process is

$$\frac{dM_z}{dt} = -(M_z - M_0)/T_1 \tag{1.11}$$

where T_1 is the longitudinal relaxation time. This process is the spin system exchanging energy with the surrounding thermal reservoir, known as the "lattice." Transverse, or spin-spin, relaxation is described by the equation

$$\frac{dM_{x,y}}{dt} = {-M_{x,y}}\Big/{T_2} \tag{1.12}$$

where T_2 is the transverse relaxation time. This process is where nuclear spins come to equilibrium between themselves, hence "spin-spin" relaxation. In addition to this flow of energy between spins, the net magnetization will also start to dephase because each spin in the spin packet feels a slightly different magnetic field and rotates at slightly different Larmor frequencies. T_1 governs the rate of recovery of the longitudinal magnetization back to thermal equilibrium and T_2 governs the rate of magnetization loss in the transverse plane.

1.2.5 Steady State Solution to the Bloch equations and Lineshapes

If we solve Eqn. 1.10 for M'_x, M'_y, and M'_z with the time derivative equal to zero, we get the steady state solutions to the Bloch equations in the rotating frame

$$M'_x = \frac{M_0 \omega_1 T_2^2 \Omega}{T_2^2 \Omega^2 + 1 + T_1 T_2 \omega_1^2} \tag{1.13}$$

$$M'_y = \frac{M_0 \omega_1 T_2}{T_2^2 \Omega^2 + 1 + T_1 T_2 \omega_1^2} \tag{1.14}$$

$$M'_z = \frac{M_0 [1 + T_2^2 \Omega^2]}{T_2^2 \Omega^2 + 1 + T_1 T_2 \omega_1^2} \tag{1.15}$$

Eqn. 1.13 is known as the dispersive mode and Eqn. 1.14 is known as the absorptive mode. The shape of the M_x' and M_y' signal when $\omega_1 \ll (T_1T_2)^{-1/2}$ is shown in Figure 1.5 and are known as Lorentzian lineshapes.

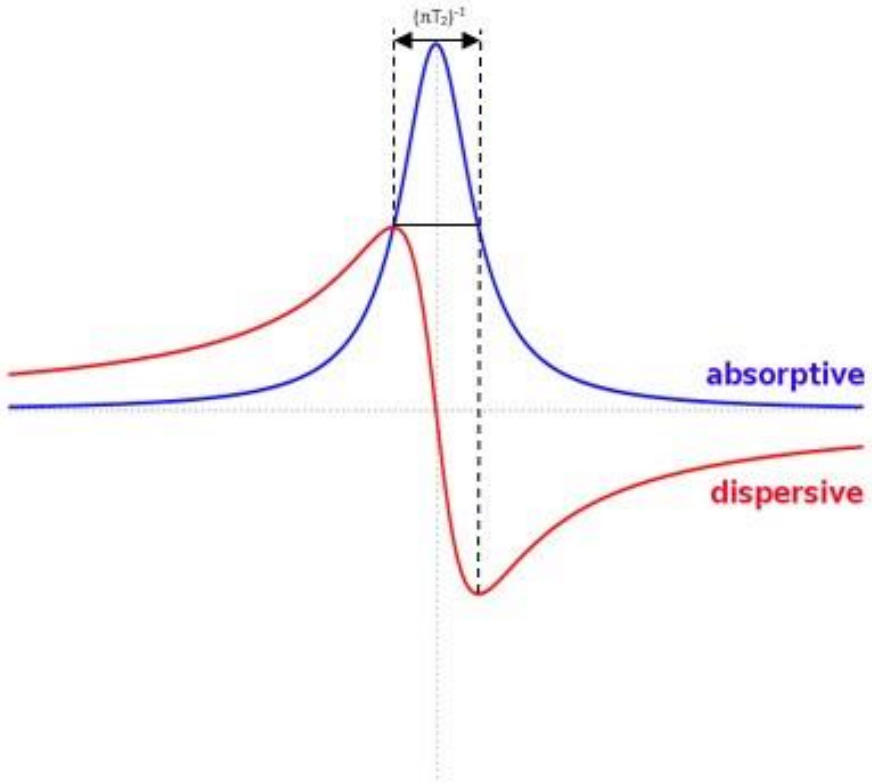

Figure 1.5. Lorentzian absorption and dispersion lineshapes predicted by the solutions to the Bloch equations (Eqn. 1.10 and 1.11.)

When the condition $\omega_1 \ll (T_1T_2)^{-1/2}$ is met, the absorption lineshape is proportional to

$$g(\nu) = \frac{2T_2}{1+4\pi^2T_2^2(\upsilon_0-\upsilon)^2} \tag{1.16}$$

where $g(v)$ is called the lineshape factor, $\omega_0 = 2\pi\upsilon_0$ and $\omega = 2\pi v$ were substituted into Eqn. 1.14 to be in frequency units. The width of the absorption line at half-height is equal to $\Delta\upsilon_{1/2} = (\pi T_2^*)^{-1}$, called the apparent T_2^*. Fig. 1.5 demonstrates the shape of an ideal experiment where the transverse relaxation is exponential and single valued. Often, the NMR signal is not truly Lorentzian due to instrumental effects such as inhomogeneity broadening. This broadening occurs because of small variations in the magnetic field strength B_0 across the dimensions of a sample. This variation leads to a mixture of lines with slightly different Larmor frequencies. The natural linewidth of the signal $(\pi T_2^*)^{-1}$ is so narrow that instrumental effects can have a large effect on the observed linewidth. To minimize the effects of field inhomogeneity, at least at high-field, the cylindrical sample tube can be spun about the z-axis to seem more homogeneous about the x and y-axis. Shimming, or altering the position of the coils, can also be used to make the B_0 field along the z-axis more homogeneous to reduce line broadening and allow the width of the lineshape to more accurately reflect the T_2^*.

1.2.6 Free Induction Decay and Fourier Transform NMR

After a 90° pulse, the net magnetization is placed in the $x'y'$ plane. Once the net magnetization is in the xy' plane, it will rotate about the $\boldsymbol{B}_0$ field (+ z-axis) at the appropriate Larmor frequency according to the nuclei of interest. As the transverse magnetization precesses about the z-axis in the transverse plane, it induces a current in the detecting coil. Plotting the induced current as a function of time results in a sinusoidal wave, which, inevitably decays due to the dephasing of the spin packets of the individual spins in the sample that all have slightly different Larmor frequencies. This plot is called the Free Induction Decay (FID). The Fourier transform (FT) of this time domain spectrum give the frequency domain equivalent. This reveals

to the observer how many different frequencies are summed together to produce the FID in the time domain.

REFERENCES

[1] Levitt M. *Spin Dynamics: Basics of Nuclear Magnetic Resonance*. John Wiley & Sons, Ltd, New York, NY, 2001.
[2] Abragam, A. *Principles of nuclear magnetism*, Clarendon Press, Oxford, NY 1961.
[3] Harris K, Robin. *Nuclear Magnetic Resonance Spectroscopy*, John Wiley & Sons, Inc, New York, NY 1989.
[4] Callaghan T, Paul. *Principles of Nuclear Magnetic Resonance Microscopy*, Oxford University Press, Oxford, NY 1991.
[5] F. Bloch, "Nuclear Induction", *Physical Review* **70**, 4604–73 (1946)

Chapter 2: NMR: A Quantum Mechanical Approach

2.1 Quantum Mechanical Description of an Ensemble of Spins

Systems observed in NMR experiments contain exceedingly large numbers of nuclear spins and must be treated statistically as an "ensemble." Significant differences between the classical approach to NMR and the quantum mechanical is that the classical approach is only valid for a collection of non-interacting spins. In addition, whenever there are equivalent spin interactions, solving the problem of finding spin parameters becomes quantum mechanical in nature because atomic nuclei are characterized by states that are inherently quantum mechanical. Individual spins do not have associated T_1 or T_2 values, only interacting spins can undergo relaxation. We therefore need a process to be able to describe real systems with all of their nuance.

2.1.1 Quantum Mechanic Basics

There are few necessary components of quantum mechanics to understand when describing nuclear magnetic resonance [1-5]. The first is the concept of a spin state which can be described by a discrete set of possibilities known as a basis set. For NMR, this basis set will be that of the angular momentum, *m*, measured along the z-axis. The angular momentum may take on values ranging from $-I,\ -I+1, \ldots, I-1, I$ where I is called the angular momentum quantum number (sometimes known as "spin") and can be a discrete set of integer or half-integer numbers. This integer is a fixed value that describes the ground state of a nucleus such as ^{1}H having a spin $I = 1/2$ or ^{6}Li having a spin $I = 1$ quantum number. In general, angular momentum has units of $\hbar$, but we will neglect explicitly writing it out unless necessary. The state of a nucleus can be written

in terms of a complete set of functions to describe any possible wave function of the system as a linear combination of basis states.

$$|\Psi\rangle = \sum_m c_m |m\rangle \tag{2.1}$$

where c_m is the coefficient of the overlap integral and can be represented as a complex value with amplitude and phase.

2.1.2 Angular Momentum and Commutation Relationships

The second concept to understand is that of the eigenvalue equation. Using angular momentum for the example observable, its eigenvalue equation for determining the angular momentum component along the z-axis looks like

$$I_z|m\rangle = m|m\rangle \tag{2.2}$$

Here, I_z is the 'operator' for angular momentum along the z-axis and m is the resultant eigenvalue. For a spin ½ nucleus, $|m\rangle$ has a discrete set of states which can be represented by the spin up state, α, and the spin down state, β. Applying the I_z operator to these states results in the eigenvalues $I_z|\alpha\rangle = +\frac{1}{2}|\alpha\rangle$ and $I_z|\beta\rangle = -\frac{1}{2}|\beta\rangle$. The Pauli matrices can be used to represent the x, y, and z components of spin in the $|\pm m\rangle$ basis for a spin ½ nucleus

$$I_x = \frac{1}{2}\begin{bmatrix}0 & 1\\ 1 & 0\end{bmatrix}, I_y = \frac{1}{2}\begin{bmatrix}0 & -i\\ i & 0\end{bmatrix}, \text{and } I_z = \frac{1}{2}\begin{bmatrix}1 & 0\\ 0 & -1\end{bmatrix}. \tag{2.3}$$

This brings us to the third concept to understand in the pursuit of understanding NMR - commutation relationships. All properties of the spin operators can be deduced from commutation relations such as

$$\begin{aligned} [I_x, I_y] &= I_x I_y - I_y I_x = iI_z \\ [I_y, I_z] &= I_y I_z - I_z I_y = iI_x \\ [I_z, I_x] &= I_z I_x - I_x I_z = iI_y. \end{aligned} \tag{2.4}$$

The square of the magnitude of the total angular momentum is represented by the operator

$$\boldsymbol{I}^2 = I_x^2 + I_y^2 + I_z^2. \tag{2.5}$$

It can be seen from Eqn. 2.4 that the I_x, I_y, and I_z operators do not commute meaning that there are no states that are simultaneous eigenstates of these operators. For example, if a spin function is in an eigenstate of I_z with eigenvalue m, then an observation of the z component of angular momentum can be determined exactly, while the x and y components would remain uncertain. The $\boldsymbol{I}^2$ operator (Eqn. 2.5), on the other hand, does commute with I_x, I_y, and I_z which means that one can determine both the magnitude of angular momentum and its component in one direction simultaneously. To navigate between states, it is useful to introduce the raising and lowering operators

$$I_+ = I_x + iI_y \text{ and } I_- = I_x - iI_y. \tag{2.6}$$

These linear combination of I_x and I_y operators change a $|+m\rangle$ state into a $|-m\rangle$ state and vice versa. Here, we have derived the properties of the spin operators through commutation relationships without having to know anything about the internal structure of the nuclei.

2.1.3 The Schrödinger Equation

The last concept to introduce for a working knowledge of quantum mechanics in its relation to NMR is that the dynamics of the system can be completely described by the *Schrödinger Equation*

$$i\hbar\frac{\partial}{\partial t}|\Psi(\mathrm{x,t})\rangle = H|\Psi(\mathrm{x,t})\rangle \tag{2.7}$$

where H is the Hamiltonian (or energy) operator

$$H = -\gamma\hbar\boldsymbol{B}_0 I_z. \tag{2.8}$$

If we consider our states to be stationary in time, we can solve the *Schrödinger Equation* as its first order differential equation to get

$$|\Psi(\mathrm{x,t})\rangle = e^{-iHt}|\Psi(\mathrm{x},0)\rangle. \tag{2.9}$$

Nuclei have a magnetic dipole moment proportional to their angular momentum, which is described by the nuclear gyromagnetic ratio, γ. The classical interaction energy between the magnetic dipole moment $\boldsymbol{\mu}$ and the magnetic field $\boldsymbol{B}_0$ is $E = -\boldsymbol{\mu}\cdot\boldsymbol{B}_0$, and the corresponding

quantum mechanical operator is the Hamiltonian above (Eqn. 2.8) where the magnetic field is pointing along the z-axis. This interaction is known as the Zeeman interaction. Now, consider a nuclear spin state $|\Psi\rangle$ under the influence of the B_0 field along the z-axis. We can see that Eqn. 2.9 becomes $|\Psi(\mathrm{x,t})\rangle = e^{-i\gamma B_0 I_z t}|\Psi(\mathrm{x},0)\rangle$. This is essentially a clockwise rotation about the z-axis by an angle $\gamma B_0 t$ where $\gamma B_0 = \omega_0$. Here, we see the similarity between the classical approach and the quantum approach to Larmor precession of a nuclei in the presence of a strong magnetic field B_0.

2.1.4 The Density Operator

So far, our quantum mechanical treatment covered the dynamics of a single spin. In reality, we deal with ensembles of spins that make up our systems and may occupy different states $|\Psi\rangle$. Our solution, therefore, needs to take into account the resulting ensemble averages. It is useful to accomplish this by introducing the spin density operator

$$\rho(t) = \overline{|\Psi\rangle\langle\Psi|} \tag{2.10}$$

where ρ is our density operator and the overbar represents an averaging over all spins in the system. An important property to note about the density operator is its ability to predict the expectation value (average over all spins) of another operator. For example,

$$\langle Q\rangle = \overline{\langle\Psi|Q|\Psi\rangle} = Tr\{\overline{|\Psi\rangle\langle\Psi|}\mathrm{Q}\} = Tr\{\rho Q\} \tag{2.11}$$

where Q is our operator corresponding to some observable, and Tr represents the trace of the matrix generated by the two operators. This is a critical component to the density operator formulation because we now have the expectation value for the entire system in terms of only two operators. If we now apply the Schrödinger equation to our density operator, we can determine its evolution in time.

$$\begin{aligned}\frac{\partial}{\partial t}\rho(t) &= \frac{\partial}{\partial t}\left(\overline{|\Psi\rangle\langle\Psi|}\right) \\ &= \left[-iH\overline{|\Psi\rangle\langle\Psi|} + i\overline{|\Psi\rangle\langle\Psi|}H\right] \\ &= -i[H\rho(t) - \rho(t)H] \\ &= -i[H, \rho(t)] \end{aligned} \tag{2.12}$$

This equation is known as the Liouville-von Neumann equation. The diagonal elements of the resulting density matrix represent the fractional populations of the spin system and the off-diagonal elements represent the coherence. The differences between fractional populations of the density matrix are the longitudinal magnetization of the system. Now, the goal is to use this awesome mechanic to predict the NMR experiment.

To do this, we will need to determine the values of the density operator. Let's do this for a spin ½ using statistical mechanics.

$$\rho_{m,n} = \frac{e^{-\frac{\hbar\omega_m}{k_b T}}}{\sum_n e^{-\frac{\hbar\omega_n}{k_b T}}} \tag{2.13}$$

where the exponential factors are $\omega_+ = +\frac{1}{2}\omega_0 = -\frac{1}{2}\gamma B_0$ and $\omega_- = -\frac{1}{2}\omega_0 = +\frac{1}{2}\gamma B_0$, and k_b is the Boltzman constant. To simplify the math let's let $\mathcal{B} = \frac{\hbar\gamma B_0}{k_b T}$ so that the exponentials are now $e^{+\frac{1}{2}\mathcal{B}}$ and $e^{-\frac{1}{2}\mathcal{B}}$. Using the small angle approximation and the high-temperature limit results in the density operator at equilibrium,

$$\rho = \begin{pmatrix} \frac{1}{2}+\frac{1}{4}\mathcal{B} & 0 \\ 0 & \frac{1}{2}-\frac{1}{4}\mathcal{B} \end{pmatrix} = \frac{1}{2}\hat{1} + \frac{1}{2}\mathcal{B}I_z. \tag{2.14}$$

The time evolution of the density operator can be obtained by applying a rotation sandwich. For example, applying a 90° pulse about the x-axis would look like

$$\rho(t_2) = R_x\left(\frac{\pi}{2}\right)\rho(t_1)R_x\left(-\frac{\pi}{2}\right) = R_x\left(\frac{\pi}{2}\right)\frac{1}{2}\hat{1} + \frac{1}{2}\mathcal{B}I_z R_x\left(-\frac{\pi}{2}\right)$$

$$\rho(t_2) = \frac{1}{2}R_x\left(\frac{\pi}{2}\right)\hat{1}R_x\left(-\frac{\pi}{2}\right) + \frac{1}{2}\mathcal{B}R_x\left(\frac{\pi}{2}\right)I_z R_x\left(-\frac{\pi}{2}\right)$$

$$\rho(t_2) = \frac{1}{2}\hat{1} - \frac{1}{2}\mathcal{B}I_y$$

$$\rho(t_2) = \frac{1}{2}\begin{pmatrix}1 & 0\\ 0 & 1\end{pmatrix} - \frac{1}{2}\mathcal{B}\frac{1}{2i}\begin{pmatrix}0 & 1\\ -1 & 0\end{pmatrix} = \begin{pmatrix}\frac{1}{2} & -\frac{\mathcal{B}}{4i}\\ \frac{\mathcal{B}}{4i} & \frac{1}{2}\end{pmatrix}. \tag{2.15}$$

We can see here how the RF pulse has equalized the diagonal elements and has introduced coherence into the system. This is equivalent to an RF pulse in the previous chapter using classical mechanics, but here, we can see how the coherence influences the system. Because we measure real systems of spin, including their interactions, it is useful to highlight the difference in the two

approaches and how the density operator can help achieve a description of a real system. The 90° pulse has moved the net magnetization into the −y-axis from the +z-axis and introduced coherence into the spin system.

Now let's see what happens to the spin system after the RF pulse has ended and is only under the effects of the B_0 field. We will use the same approach and apply the evolution operator to the density matrix $\rho(t_2)$.

$$\rho(t_3) = R_z(\Omega_0\tau)\left(\frac{1}{2}\hat{1} - \frac{1}{2}\mathcal{B}I_y\right)R_z(-\Omega_0\tau) = \frac{1}{2}\hat{1} - \frac{1}{2}\mathcal{B}R_z(\Omega_0\tau)I_yR_z(-\Omega_0\tau)$$

$$\rho(t_3) = \frac{1}{2}\hat{1} - \frac{1}{2}\mathcal{B}\left(I_y cos(\Omega_0\tau) - I_x sin(\Omega_0\tau)\right)$$

$$\rho(t_3) = \frac{1}{2}\hat{1} - \frac{1}{2}\mathcal{B}\frac{1}{2i}\begin{pmatrix} 0 & e^{-i\Omega_0\tau} \\ e^{+i\Omega_0\tau} & 0 \end{pmatrix}$$

$$\rho(t_3) = \frac{1}{2}\hat{1} - \frac{\mathcal{B}}{4i}e^{-i\Omega_0\tau}I_+ + \frac{\mathcal{B}}{4i}e^{+i\Omega_0\tau}I_- \qquad (2.16)$$

where $\tau = t_3 - t_2$ and Ω_0 is the offset frequency. We can see that the populations did not change, while the coherences picked up a time-dependent phase factor.

At this point, one could use the tools demonstrated thus far to develop a NMR pulse sequence from start to finish which would describe the state of the system at any given moment. To summarize what has been exhibited so far: magnetization is derived from angular momentum, the net magnetization is the differences in fractional populations of our spin states, manipulating the density operator using RF pulses or the time evolution operator lead to a time-dependent oscillatory behavior of the transverse magnetization (coherences) which can be represented with angular momentum operators, and that signal detection is just the observation of the precession of the spins.

The NMR detector is generally setup to detect the time varying signal along the x-axis. For this setup, the desirable observable is $\langle I_x \rangle = Tr\{\rho I_x\}$. Because I_x has I_+ and I_- components, seen by rearranging Eqn. 2.6, we can discern that $\langle I_x \rangle$ is proportional to the off-diagonal elements of the density matrix (off-diagonal elements can be represented by ρ_{+-} and ρ_{-+}). The NMR signal is generally detected as the -1 coherence, which is essentially the ρ_{-+} matrix element of the density matrix. The detectable signal is proportional to $S(t) = 2i\rho_{-+}(t)e^{-i\phi_{rec}}$ where ϕ_{rec} is just the phase that the receiver is set to. What is important here is that the precession of $\rho_{-+}(t)$ can give a prediction of the expected signal called the Free Induction Decay (FID). For a more realistic prediction, we must account for relaxation, just as we did with the classical approach. The $\rho_{-+}(t)$ coherence evolves as $\rho_{-+}(t_2) = \rho_{-+}(t_1)e^{(i\Omega_0 - \frac{1}{T_2})\tau}$ when adding the relaxation term. The spin operators evolve as $I_x = (I_x \cos(\Omega_0\tau) + I_y \sin(\Omega_0\tau))e^{-\tau/T_2}$ and $I_y = (I_y \cos(\Omega_0\tau) - I_x \sin(\Omega_0\tau))e^{-\tau/T_2}$ when including relaxation. The fractional populations evolve as $\rho_{++}(t_2) = \left(\rho_{++}(t_1) - \rho_{++}^{eq}\right)e^{-\tau/T_1} + \rho_{++}^{eq}$ and $\rho_{--}(t_2) = (\rho_{--}(t_1) - \rho_{--}^{eq})e^{-\tau/T_1} + \rho_{--}^{eq}$.

We now have the full picture of the quantum mechanical approach to NMR; from angular momentum to the spin density operator and how that generates a real signal including relaxation. Using the tools described in this chapter makes it possible to take a pulse sequence from start to finish and get a predicted signal making this quite a powerful tool for the spectroscopist.

REFERENCES

[1] CHE 216 Course Notes (Matthew Augustine, UC Davis).
[2] CHE 216 Course Notes (Dylan Murray, UC Davis)
[3] Harris K, Robin. *Nuclear Magnetic Resonance Spectroscopy*, John Wiley & Sons, Inc, New York, NY 1989.
[4] Poole, Charles P., and Horacio A. Farach. *Theory of Magnetic Resonance*, Second edition. New York: Wiley, 1987.
[5] Hore, P. J., Jones, J. A., Wimperis, S. *NMR: The Toolkit*, Oxford University Press, 2015.

Chapter 3: Relaxation

3.1 Introduction

Relaxation is the process by which nuclear spins return to equilibrium. It can essentially be thought of as a process by which energy is allowed to flow between spins and molecular motion. Relaxation occurs in a real spin system where the spins can interact with each other. You cannot have relaxation for an isolated spin. Equilibrium describes the state at which the populations of energy levels are those predicted by Boltzmann statistics. Equilibrium is also when there is no transverse magnetization, or more generally, no coherences present in the spin system.

3.2 Origins of Spin Relaxation

A nucleus in a liquid will experience a random fluctuating field due to the magnetic moments of nuclei of other molecules as they execute Brownian motion. This randomly fluctuating field can be resolved by Fourier analysis into terms oscillating at different frequencies. These components can be further subdivided into elements parallel and perpendicular to the static magnetic field, B_0.

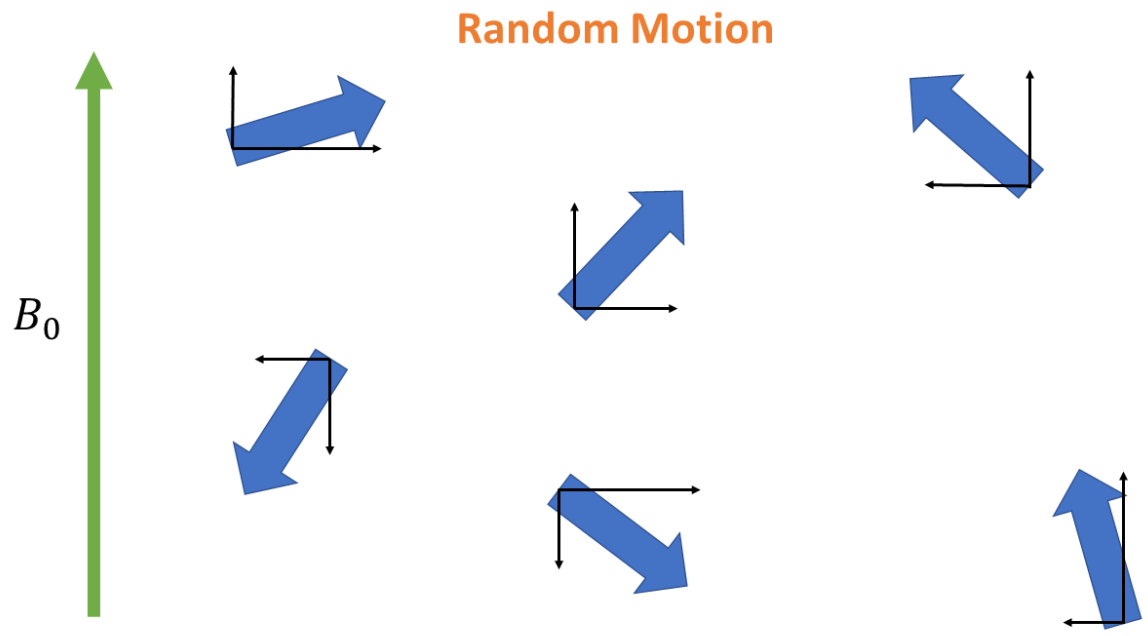

Figure 1. A graphic of a system of spins in a static magnetic field, B_0, where the magnetic moment vector is broken up into parallel and perpendicular components.

The component perpendicular to the static field, $B_{0\perp}$, which oscillates at the Larmor frequency induces transitions between energy levels given that the energy corresponds to the Zeeman splitting of the nuclei of our system. The population of the states relax back to Boltzmann equilibrium and is described by T_1, the relaxation of the longitudinal component of the net magnetization, $\boldsymbol{M}$.

$B_{0\perp}$ also affects T_2 in addition to the parallel component, $B_{0\parallel}$. To illustrate this notion, from the uncertainty principle we know that $\Delta E = {\hbar}/{\Delta t}$, where Δt represents the lifetime of the states. The lifetime of the states is reduced by random fluctuations of the local magnetic field. Therefore, fluctuations that induce transitions between states also increase linewidth associated with the transverse relaxation, T_2, as seen in Ch. 1 where the width at half-height is equal to $\Delta\upsilon_{1/2} =$

$(\pi T_2^*)^{-1}$. The other contribution comes from the fluctuations in the z-direction which relate directly to variations in the total magnetic field in the z-direction, and hence, linewidths.

3.3 Theory of Relaxation

If relaxation is the process by which spins return to equilibrium, then let us start by describing equilibrium mathematically (for a spin ½ particle). Equilibrium magnetization arises from the unequal populations of the two states that correspond to the α and β spin states. M_z is proportional to the population difference,

$$M_z \propto (N_\alpha - N_\beta) \propto n \tag{3.1}$$

where we will let $n = N_\alpha - N_\beta$ and $N = N_\alpha + N_\beta$. If the populations at some time, t, are not in equilibrium, then for the system to reach equilibrium the populations of one state must decrease and that of the other must increase. This implies that there must be transitions between the two levels. Next, we will assume that the rate of transition is proportional to the population of the state and is a first-order process with rate constant, W. The rate of decreasing population for the α state is therefore W_α and for the β state, W_β. The change in population difference is then,

$$\frac{\partial}{\partial t} n = \frac{\partial}{\partial t} N_\alpha - \frac{\partial}{\partial t} N_\beta \tag{3.2}$$

and plugging in $\frac{\partial}{\partial t} N_\alpha = -W_\alpha N_\alpha + W_\beta N_\beta$ and $\frac{\partial}{\partial t} N_\beta = -W_\beta N_\beta + W_\alpha N_\alpha$ into Eqn. 3.2 we get

$$\frac{\partial}{\partial t}n = N(W_\beta - W_\alpha) - n(W_\alpha + W_\beta). \tag{3.3}$$

If we then factor out $-(W_\alpha + W_\beta)$ and let $N\left(\frac{W_\beta - W_\alpha}{W_\alpha + W_\beta}\right) = n_0$ then we get,

$$\frac{\partial}{\partial t}n = -\frac{1}{T_1}(n - n_0) \tag{3.4}$$

where $T_1^{-1} = W_\alpha + W_\beta$ and n_0 represents an equilibrium magnetization. Eqn. 3.4 relates the change in magnetization to the longitudinal relaxation. What remains to be determined are the rate constants, W.

3.3.1 Time Dependent Perturbation Theory

To help us determine the rate constants, we will turn to the ever-valuable perturbation theory. Suppose we have a spin system governed by the following Hamiltonian

$$H = H_0 + V(t) \tag{3.5}$$

where the potential function, $V(t)$, is assumed to be small relative to H_0. This Hamiltonian will have both diagonal and off-diagonal matrix elements. Continuing with our spin ½ system with states $|\alpha\rangle$ and $|\beta\rangle$, and energies E_a and E_b perturbed by the potential, $V(t)$. The diagonal elements of $\int \Psi_i^* V \Psi_j^* d\tau = V_{ij}$ corresponding to V_{aa} and V_{bb} cause the time-dependent fluctuations in the energies E_a and E_b while the off-diagonal elements induce transitions between them. The time-dependent *Schrödinger Equation* (Eqn. 2.7) has the solution,

$$\Psi = c_a(t)\Psi_a e^{-\frac{iE_a t}{\hbar}} + c_b(t)\Psi_b e^{-\frac{iE_b t}{\hbar}}. \tag{3.6}$$

The coefficients c_a and c_b satisfy the equations

$$i\hbar\frac{\partial}{\partial t}c_a = f(t)e^{i(E_a - E_b)t/\hbar}V_{ab}c_b \tag{3.7}$$

$$i\hbar\frac{\partial}{\partial t}c_b = f(t)e^{i(E_b - E_a)t/\hbar}V_{ba}c_a. \tag{3.8}$$

Let the system be in the ground state at $t = 0$ so that $c_a(0) = 1$ and $c_b(0) = 0$. Then the probability of a transition from state $|\alpha\rangle$ to $|\beta\rangle$ at time $t > 0$ is,

$$\begin{aligned} P_{a\to b} &= |c_b(t)|^2 \\ &= \left(\tfrac{|V_{ab}|^2}{\hbar^2}\right)\int_0^t dt' \int_0^t dt'' \, f(t')f(t'')e^{iW_{ba}(t'-t'')} \\ &= \left(\tfrac{|V_{ab}|^2}{\hbar^2}\right)\int_0^t dt' \int_{-t'}^{t-t'} d\tau \, f(t'+\tau)f(t')e^{iW_{ab}\tau}. \end{aligned} \tag{3.9}$$

$P_{a\to b}$ represents the probability of a transition between the $|\alpha\rangle$ and $|\beta\rangle$ states. Now the question is what does the $\int_0^t dt' \int_{-t'}^{t-t'} d\tau \, f(t'+\tau)f(t')e^{iW_{ab}\tau}$ piece represent? For this, we will transition into an explanation of correlation functions.

3.3.2 Correlation Functions

The behavior of random fluctuations can be described by a correlation function. For random thermal motion, the ensemble average tends to zero since the function is distributed around zero. Yet, an important property of random functions is the correlation function, $G(t,\tau)$.

$$G(t,\tau) = F_1(t)F_1^*(t+\tau) + F_2(t)F_2^*(t+\tau) + \cdots$$
$$= F(t)F^*(t+\tau) \qquad (3.10)$$

$F_1(t)$ is the field experienced by spin one at time t, and $F_1^*(t+\tau)$ is the field experienced at a time τ later. Eqn. 3.10 here should look familiar since it has the same structure as the integral piece from Eqn. 3.9 signifying that it is, in fact, a correlation function.

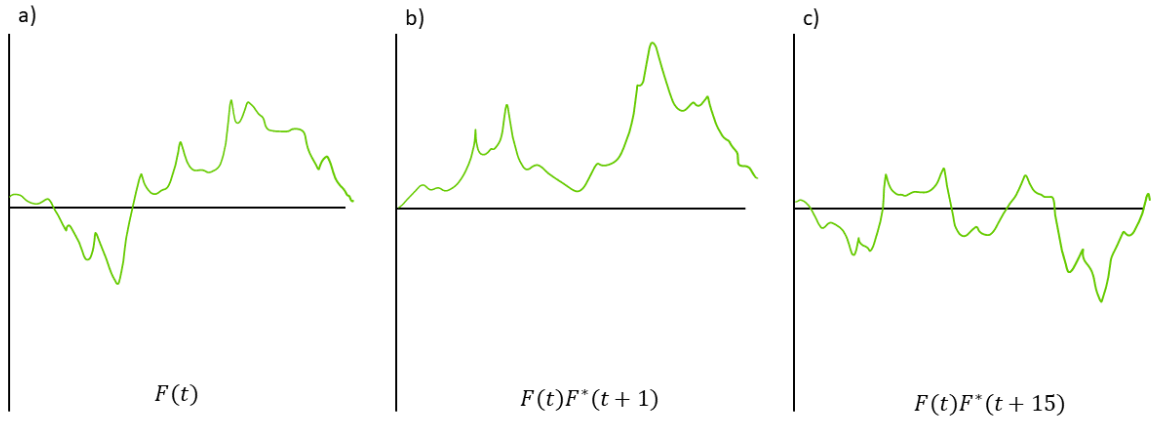

Figure 2. Plot of the correlation function at (a) some time t, (b) at some time t plus some time τ, and (c) some time t plus a longer time τ. These plots act as a visual representation of how at longer τ times, the average of the area goes to zero. For shorter τ times, there is a non-zero area.

We can see here, in the limit as $\tau \to \infty$, $G(t,\tau) \to 0$, but for shorter time steps we have a non-zero area. As a note, we can also write the correlation function as just $G(\tau)$ for a stationary function. This function, $G(\tau)$, is a function that characterizes the "memory" that the system has of a particular arrangement of spins in the sample. The simplest form of $G(\tau)$ is

$$G(\tau) = G(0)e^{-|\tau|/\tau_c} \tag{3.11}$$

where τ_c is the correlation time. The correlation time can be thought of as the time it takes a molecule to rotate through one radian.

3.3.3 Spectral Density Function

The correlation function, $G(\tau)$, is a function of time and can therefore be Fourier transformed to achieve its equivalent in the frequency domain. The Fourier transform of the correlation function results in the spectral density function which gives a measure of the amount of motion present at different frequencies. For the simple exponential correlation function given in Eqn. 3.11, the corresponding spectral density function is,

$$J(\omega) = \int_{-\infty}^{\infty} G(\tau)\, e^{-i\omega\tau} d\tau$$

$$e^{-\tau/\tau_c} \xrightarrow{FFT} \frac{2\tau_c}{1+\omega^2\tau_c^2}$$

$$J(\omega) = \frac{2\tau_c}{1+\omega^2\tau_c^2}. \tag{3.12}$$

Now we have all the pieces necessary to describe the transition probability rate which in turn tells us what the relaxation rates are.

$$W = P_{a\to b} = \frac{1}{\hbar^2}|V_{ab}|^2 \frac{2\tau_c}{1+\omega^2\tau_c^2} \tag{3.13}$$

where $V_{ab} = \langle b|V|a\rangle$ and $V_{ab} = {V_{ba}}^*$ from Eqn. 3.9. The math is the same for $P_{b\to a}$, so

$$T_1^{-1} = 2W = \frac{2}{\hbar^2}|V_{ab}|^2 J(\omega). \tag{3.14}$$

The $B_{0\perp}$ contributions require a fluctuating field and thus depends on $J(\omega)$. The $B_{0\parallel}$ contribution involves no energy change, so the spectral density function is $J(0)$, leaving the expression

$$T_2^{-1} = (2T_1)^{-1} + \frac{1}{2}|V_{ab}|^2 J(0) \tag{3.15}$$

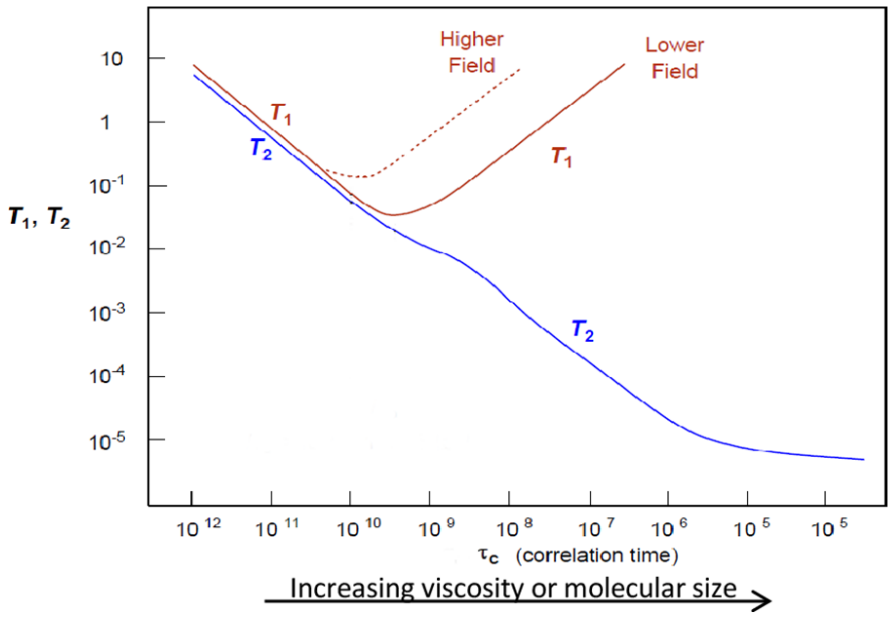

Figure 3. Plot of T_1 and T_2 versus correlation time, τ_c. Exemplifies the progression of the different relaxation times as the correlation time decreases.

We can see in Fig. 3 that as the correlation time increases, the value of T_1 decreases before plateauing as $\tau_c = 1/\omega_0$, and then increasing again. In comparison, T_2 continually decreases because the spectral density function is $J(0) = 2\tau_c$, so as τ_c decreases, T_2 decreases.

REFERENCES

[1] Bloembergen, N., Purcell, E. M., and Pound, R. V. (1948). *Phys. Rev*, **73**, 679.
[2] Harris K, Robin. *Nuclear Magnetic Resonance Spectroscopy*, John Wiley & Sons, Inc, New York, NY 1989.
[3] Poole, Charles P., and Horacio A. Farach. *Theory of Magnetic Resonance*, Second edition. New York: Wiley, 1987.

Chapter 4: Investigating Lithium-ion Polymer Batteries using Relaxometry and Magnetic Resonance Imaging

Abstract

Advancements in battery technology are important for the growth of markets such as portable electronics, energy storage and electric vehicles. Accompanying the rise of lithium battery technology is the need for fast, non-destructive diagnostic techniques to determine important battery parameters that will define a batteries functionality or performance. Low-field NMR is an ideal technique to probe lithium-ion polymer (LiPo) batteries due to the ability to penetrate the aluminum casing of these batteries. The development of a few different techniques are presented here to measure different battery parameters. This includes measuring the T_1 and T_2 parameters of LiPo batteries at differing states of charge, magnetic resonance imaging to provide images showing T_2 as a function of position across a battery, and using pulsed field gradient ^{7}Li nuclear magnetic resonance (NMR) to measure Li diffusion coefficients.

4.1 Introduction

Lithium-ion batteries (LIBs) play a critical role in the advancement of portable electronic technologies and have recently entered the automobile industry with the advent of electric vehicles. LIBs have a high volumetric energy density and a low self-discharge rate making them a desirable choice for any modern-day electronics [1]. Lithium-ion polymer (LiPo) batteries are a subcategory of LIB's that use a polymer gel as an electrolyte instead of an aqueous liquid making them a safer option since there is less pressurized flammable liquid electrolyte available to ignite. The battery construction includes dissolving the lithium salt into a high-molecular-weight polymer such as

polyethylene oxide (PEO) sandwiched between the electrodes of the cell. The whole cell is held within a laminated aluminum casing [2]. The increasing demand for LiPo batteries has driven development of both electrode materials and electrolyte media in the continued search to improve energy capacity and performance safety.

The electrolyte is a crucial component in battery performance since its main function is to conduct ions. This function dictates how quickly stored energy from the electrodes can be dispensed to the load. Therefore, it is important to investigate and optimize the transport properties of the electrolyte in a battery allowing for more current draw. Another issue of importance is lithium microstructure formation. Upon excess charging of the cell, lithium metal can build up on the anode and cause short circuiting and capacity loss. One study here will focus on investigating electrolyte dynamics by measuring diffusion coefficients and ion transference numbers of Li and F. This can be achieved by using pulsed field gradient spin echo ^{7}Li and ^{19}F NMR pulse sequences to obtain information on the lithium species in the LiPo battery.

Pulsed field gradient-NMR (pfg-NMR) and electrochemical methods have been used to determine diffusion coefficients and ion transference numbers in mixed-gel electrolytes previously [3]. ^{7}Li NMR has also been used on specifically deconstructed electrode or bag cell materials to attempt quantification of lithium microstructure formation [4,5]. However, neither of these investigations were applied to commercially ready LiPo batteries because the conductive metal casing is a barrier to all but the lowest frequencies of electromagnetic radiation. This is due to the attenuation of the radio frequency (RF) field through a conductive surface, such as the aluminum casing of a LiPo battery, shown in the skin depth equation

$$\delta = \sqrt{\frac{2\rho}{\mu\omega}} \tag{4.1}$$

where $\rho$is the resistivity of the metal, $\mu = \mu_0\mu_r$ where $\mu_0$is the vacuum permeability, $\mu_r$is the relative permeability of the metal (aluminum casing), ω is the frequency (rad/s) of the applied RF field, and $\delta$is the skin depth. Skin depth is the distance an electromagnetic wave can penetrate into a conductive medium before decaying to a value of $1/e$ of the original amplitude. Skin depth is inversely proportional to the frequency of the applied radio frequency field, consequently, operating at low frequencies results in an increased penetration depth.

The goal of this research is to determine the most accurate values of diffusion coefficients and ion transference numbers by investigating LiPo batteries in action (in situ). Diffusion coefficients describe the ability of a species to move through a medium and the cation transference number (t_i) is a fraction of the total current carried in the electrolyte by the cation species as seen in Eqn. 4.2,

$$t_i = \frac{D_+}{D_+ + D_-} \tag{4.2}$$

where D_+ is the diffusion coefficient of the cation species and D_- is the diffusion coefficient of the anion species. As of yet, nearly all relevant data has been achieved by specially constructing bag cells or using solutions in tubes so the skin depth problem can be avoided. While that work provided good approximation, the electrolyte in a commercial pouch cell will occupy a different environment and therefore needs to be properly tested for the most accurate data. Pfg-NMR was

used on $CuSO_4$ in water to determine ideal pulse lengths, gradient strengths and to solidify proof of concept measuring diffusion coefficients.

Another facet of research accomplished in this study was using low-field NMR to determine relaxation times as a function of the state of charge of a LiPo battery. The low field which was used in this study ensures RF penetration across the metal into the battery resulting in detectable proton signal in relatively few scans. The NMR relaxometry parameters T_1 and T_2 yield information about the bulk macroscopic properties of a system. Here, the T_1 and T_2 parameters are used to analyze LiPo batteries at differing states of charge and magnetic resonance (MR) imaging is used as another method to image a LiPo battery to screen for lithium microstructure formation.

4.2 Experimental

To accommodate the unique geometry of LiPo batteries in production a customized probe coil was built to house the PGEB – NM053040 model LiPo battery with 3.7 V nominal voltage and 600 mAh capacity studied here.

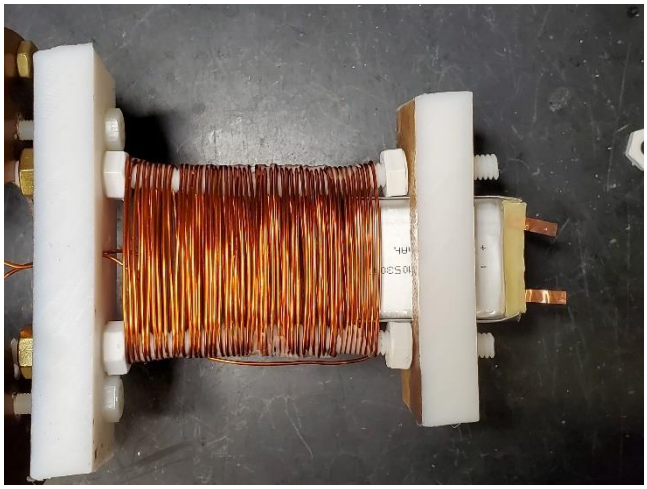

Figure 1: Probe coil containing a lithium-ion polymer battery.

For the experiment measuring relaxation parameters, the probe/battery setup shown in Fig. 1 was placed into the homogeneous region of an electromagnet powered by a DANFYSIK System 8000 Magnet Power Supply at 23.02 amps generating a 53.2 mT B_0 field corresponding to a ^1H Larmor frequency of 2.265 MHz. A Tecmag Redstone spectrometer and integrated TNMR software were used for the relaxation experiments.

A free induction decay (FID) signal was recorded using a 90° pulse time of 20 μs. Obtaining ^1H signal from the FID substantiated the idea that working at 2.265 MHz ^1H Larmor frequency offers enough skin depth penetration to reach the electrolyte (source of protons) in the LiPo battery. Once signal was proven attainable, T_2 measurements were acquired using a Carr-Purcell-Meiboom-Gill (CPMG) pulse sequence with 200 echoes and repeated at different states of charge. The resulting echo train was fit to the exponential decay

$$S(t) = S_1 e^{-t/T_{2,short}} + S_2 e^{-t/T_{2,long}}. \quad (4.3)$$

where S_1 and S_2 are the amplitudes and S(t) is the signal at any later time. T_1 measurements were acquired using a saturation recovery pulse sequence at different states of charge and fit to

$$S(t) = S_0(1 - e^{-t/T_1}). \quad (4.4)$$

All data fitting was performed using cftool native to Matlab R2019a.

A spin echo sequence where the gradient was turned on along one direction was used to provide spatial resolution to enable imaging of the LiPo battery to set precedent. Once viable, the spin echo sequence was altered to a CPMG pulse sequence with a gradient which provided the images seen in Figure 3. The slice captured by the gradient pulse spans the distance of the battery. Based on the strength of the gradients, the distance across a LiPo battery can be calculated. An AE Techron Precision Industrial amplifier was used for the gradients.

For the experiment to obtain ^{1}H diffusion coefficients, the probe setup shown in Fig. 1 was placed into the homogeneous region of an electromagnet powered by a DANFYSIK System 8000 Magnet Power Supply at 21.02 amps generating a 48.6 mT B_0 field corresponding to a ^{1}H Larmor frequency of 2.07 MHz. The Tecmag Redstone spectrometer and integrated TNMR software were also used for the diffusion experiments.

As a proof of concept, a row of six 5 mm NMR tubes were filled with a 20 mM solution of $CuSO_4$ in water and placed into the probe. The water diffusion data was acquired at a Larmor frequency of 2.07 MHz with a 90° pulse of 15.1 μs. A pulsed field gradient spin echo (PFGSE) sequence was used to determine the diffusion coefficient of protons in the sample. The attenuated signal was integrated and fit to the equation,

$$\ln\left(\frac{S(t)}{S(0)}\right) = -\gamma^2\delta^2 g^2 D(\Delta - \frac{\delta}{3}) \tag{4.5}$$

where γ is the gyromagnetic ratio, δ is the length of the gradient pulses, Δ is the duration time between the pulses, gis the gradient strength, and D is the diffusion coefficient. A plot of the natural log of the signal versus the gradient squared gives a slope which depends on the diffusion

coefficient. The gradient strength was determined using a gradient spin echo pulse sequence, measuring the spectrum signal width, and applying the known width of the NMR tubes.

4.3 Results and Discussion

T_1 and T_2 measurements as a function of the state of charge are shown in Fig. 2. The T_1 and T_2 times do not vary appreciably while staying within the normal charging limits, but if the LiPo battery is over-discharged, a change in T_1 and T_2 times can be observed.

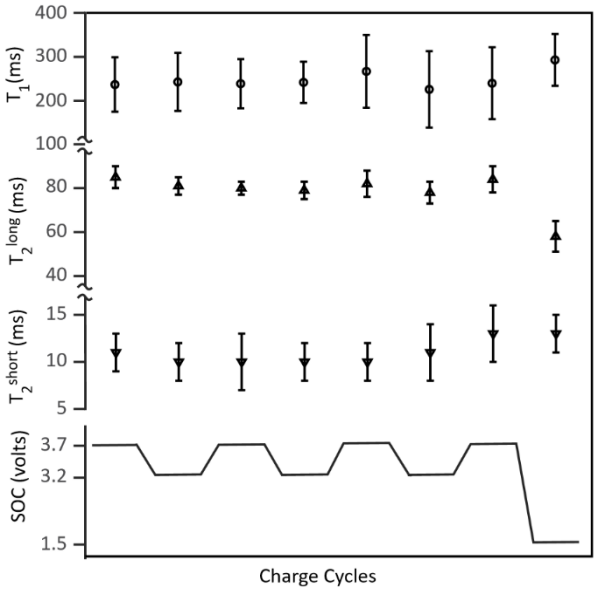

Figure 2. Plot of T_1 and T_2 values at differing states of charge of a LiPo battery. T_2 has a short and long component owing to its biexponential character.

The decrease in T_2 and increase in T_1 suggests that the correlation time, τ_c, is increasing past that of the extreme narrowing limit. T_1, however, is only inversely proportional to $\tau_c$until after the extreme narrowing limit where it becomes directly proportional (See Fig. 3 in Ch. 3). The

increase in correlation time could be due to inhibition of molecular motion in the electrolyte due to the influx of other species of molecules from the electrodes during over-discharging. Over-discharging can cause supersaturation of $LiCoO_2$, leading to the formation Li_2O in the electrolyte solution resulting in more restricted motion of the electrolyte [6].

The CPMG data yields the T_2 parameters as a function of that position across the battery. Recording T_2 values across a LiPo battery could provide information about the plating of lithium metal onto the anode during charging. If lithium ions form on an electrode, creating protruding formations, electrolyte in proximity would be impeded, changing the correlation time, therefore changing T_2 times. Depending on the axis that a gradient is applied, a T_2 change could be seen based on this microstructure formation.

The gradient CPMG pulse sequence enabled spatially resolved determination of T_2. An image of T_2 times as a function of position along an axis of the battery is shown in Fig. 3.

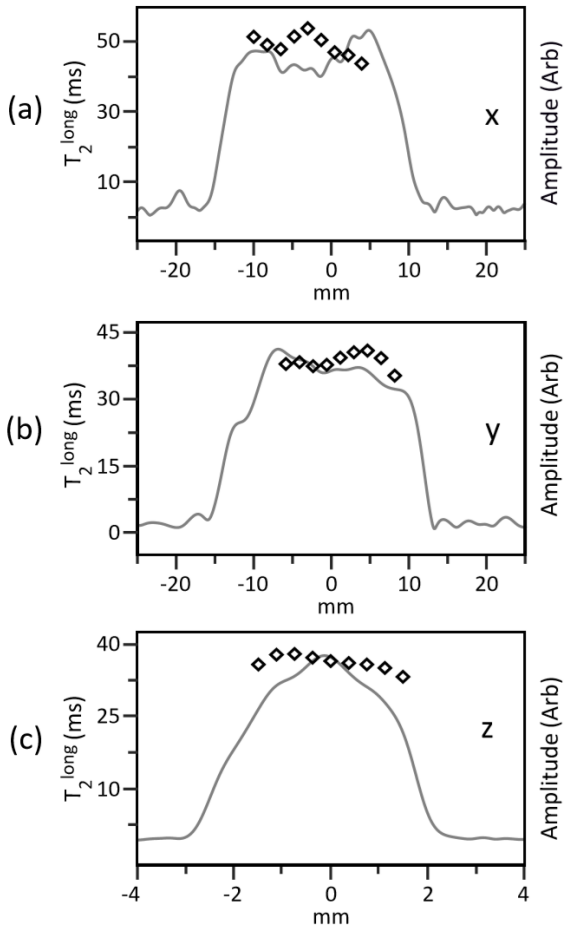

Figure 3. Long component of the T_2 times recorded as a function of position along the x, y, and z axis respectively of the LiPo battery. The gray lines in each plot are 1 dimensional 1H images across the LiPo battery.

The gradient strength was measured using a PGSE on the six NMR tubes. A range from zero to 0.8 percent of the maximum gradient strength was utilized in this experiment. The values for the x-axis span from 0.1835 G/cm to 1.4335 G/cm, the y-axis spans 0.3297 G/cm to 1.9754 G/cm, and the z-axis values span from 0.1223 G/cm to 0.7187 G/cm. Pfg-NMR was then used to determine the diffusion coefficient of a copper sulfate solution in one dimension. A plot of the natural log of the normalized signal versus the gradient strength squared is shown in Figure 4.

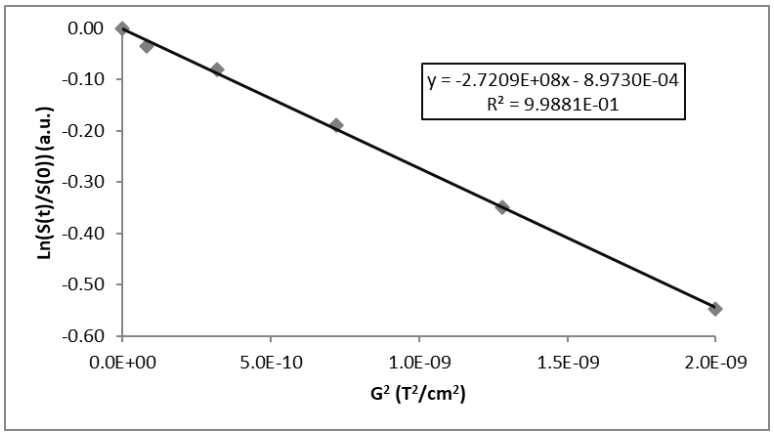

Figure 4. Plot of the natural log of the signal using pfg-NMR versus the gradient squared. The slope is then used to determine the diffusion coefficient, D.

Although Fig. 4 shows the linear relationship between the natural log of the signal and the gradient strength squared, the estimated diffusion coefficient was several orders of magnitude larger than expected. This is likely due to the fact that the $CuSO_4$ concentration was too high forcing T_1 and T_2 to be on the millisecond experimental time scale. The experiments are now being repeated with a lower $CuSO_4$ concentration with longer T_1 and T_2 values.

4.4 Conclusion

Quantifying lithium microstructure formation in commercial ready batteries has been a topic of interest for researchers previously with no success. Imaging LiPo batteries using a CPMG pulse sequence with a gradient to provide spatial resolution could produce information about lithium microstructure formation around the electrodes based on T_2 mapping. NMR relaxometry can discern between a normally functioning LiPo battery and that of an over-discharged LiPo battery by its T_1 and T_2 times and their change according to an increase in correlation times.

Pulsed field gradient NMR at low field is suitable to investigate electrolyte transport properties including diffusion coefficients. These techniques can provide valuable information on the properties of lithium-ion polymer batteries for researchers and manufacturers alike.

REFERENCES

[1] Armand, M.; *et. al. Nature* **451,** 652–657 (2008).
[2] Orsini, F. *et al. J. Power Sources* **1998**, 76, 19-29.
[3] Chauvin, C.; *et. al. Electrochim. Acta* **52** 1240 (2006).
[4] Grey, C.; *et. al. J. Phys. Chem.* **2015**, 119, 16443-16451.
[5] Jerschow, A.; *et. al. Nat. Commun.* **2018**, 9, 1766.
[6] Choi, H. C.; *et al*. *J. Phys. Chem. B.* **2003,** 107 (24): 5806-5811.